COMPDYN 2013
4th ECCOMAS Thematic Conference on
Computational Methods in Structural Dynamics and Earthquake Engineering
M. Papadrakakis, N.D. Lagaros, V. Plevris (eds.)
Kos Island, Greece, 12–14 June 2013

A COMPARISON OF TWO ELASTIC-PLASTIC APPROACHES TO CYCLIC SOIL MODELLING

Federico Pisanò[1], **Boris Jeremić**[2]

[1,2]1 University of California Davis
1 Shields Avenue 95616 Davis, California (USA)
e-mail: fpisano, jeremic@ucdavis.edu

Keywords: Geotechnical Earthquake Engineering, Soil Dynamics, Constitutive Modeling, Elasto-plasticity, Stiffness Degradation, Damping.

Abstract. *The choice of the soil constitutive relationship is an important step in the numerical modelling of many Geotechnical Earthquake Engineering problems. Although relevant results have been achieved in the field of elastic-plastic constitutive soil modelling, many practical problems are still tackled through 1D visco-elastic models, only based on shear modulus reduction and material damping curves. This is partly motivated by the usual lack of experimental data and the related difficulties in the calibration of advanced soil models. Even though the number of material parameters is kept low, multiple options exist in terms of theoretical framework for the model formulation. In this paper, the cyclic performances of two different kinematic hardening frictional models are compared. Both the models are characterized by a Drucker-Prager-type pressure-sensitiveness and non-associativeness, but, while the former is formulated as a standard elastic-plastic model with Armstrong-Frederick rotational hardening, the latter has been recently developed in the framework of bounding surface plasticity with vanishing elastic region. In particular, the bounding surface model allows for soil plastification at any load level, extending to frictional materials the previous cohesive version by Borja and Amies (1994).*

Although the two models are characterized by similar analytical structures and the same number of material parameters, the cyclic performance of the bounding surface model is apparently the most satisfactory in terms of simulated stiffness degradation and damping curves, which can be readily exploited for the calibration of the hardening parameters. The dissipation properties of both models are investigated in conjunction with an additional viscous mechanism, exploitable to improve the simulation of the experimental damping.

The effectiveness the bounding surface model is further analysed against the influence of the initial confining pressure. In particular, it is shown that the simple introduction of pressure-dependent hardening parameters readily allows to reproduce the soil cyclic response over a wide range of confining pressures.

1 INTRODUCTION

Geotechnical Earthquake Engineering (GEE) represents an important application field for Computational Dynamics methods, which have been increasingly employed in the last decades to analyse more and more challenging seismic soil-structure interaction (SSI) problems. Since SSI problems concern – by definition – both man-made structures and the interacting soil-like geomaterials, it is self-evident that no realistic results can be obtained from numerical simulations if the mechanical behaviour of all the materials involved is not properly described. In particular, modelling the mechanical response of soils is still a quite open issue because of the simultaneous presence of non-linearity, irreversibility, anisotropy and proneness to instability – especially when cyclic/dynamic loading conditions are applied to multiphase materials (i.e. filled with interstitial pore fluid(s)) [8].

The incorporation of suitable (multiaxial) constitutive relationships for soils into 3D SSI analyses is apparently a premise for reliable results to be obtained, but, on the other side, this also obstructs the routinary use of numerical methods for practical engineering purposes. Indeed, despite the huge steps forward taken in the elastic-plastic modelling of geomaterials, the most successful models in literature (overviews are given by [8, 13]) are usually characterized by rather complex analytical formulations and a quite high number of constitutive parameters: while the former aspect may result in cumbersome implementations into numerical codes and/or several computational difficulties, the latter prevents an easy model calibration on the basis of the few experimental data usually available. For these reasons, practitioners often prefer using so-called 1D equivalent linear visco-elastic models, only accounting for the dependence of the (secant) stiffness and the (viscous) damping on the cyclic strain amplitude [9].

The above considerations highlight the need for further research efforts in the field of soil cyclic modelling, not just aimed at conceiving new sophisticated constitutive relationships, but also at achieving reasonable accuracy with a minimum number of material parameters. In the present paper, this problem is addressed from a peculiar perspective, in order to point out how relevant is the choice of the theoretical/constitutive framework for the formulation of a specific soil model. For this purpose, two different elastic-plastic models are considered and compared in terms of analytical structure and resulting cyclic performance. Both the models are characterized by a Drucker-Prager-type pressure-sensitiveness and similar non-associated flow rules, but, while the former is formulated as a standard elastic-plastic model with Armstrong-Frederick rotational hardening, the latter has been recently developed in the framework of bounding surface plasticity with vanishing elastic domain [11]. In particular, the bounding surface model allows for soil plastification at the very onset of loading, extending to frictional materials a concept previously introduced by [2, 5] for the purely cohesive case.

Although the two models are characterized by similar analytical structures and – importantly – the same number of parameters, the bounding surface model appears to be preferable in terms of simulation of stiffness degradation and damping curves – here analytically implemented according to the proposal by [7]. The damping performance of both models is also investigated in conjunction with an additional viscous mechanism, exploitable to improve the simulation of the experimental damping. Finally, the initial version of the bounding surface model is slightly modified to accurately reproduce the soil cyclic response over a wide range of confining pressures.

2 CONSTITUTIVE FORMULATIONS

Hereafter, the analytical formulations of both the elastic-plastic models considered in this work are detailed. Then, the possibility of improving the purely frictional (elastic-plastic) dissipative performance through the coupling with a parallel viscous mechanism is illustrated.

Index tensor notation is henceforth used, along with the standard Einstein convention for repeated indices; the norm of any second–order tensor x_{ij} is defined as $\|x_{ij}\| = \sqrt{x_{ij}x_{ij}}$, whereas the deviatoric component can be extracted as $x_{ij}^{dev} = x_{ij} - x_{hk}\delta_{hk}\delta_{ij}/3$ (δ_{ij} is the Kronecker delta). In accordance with usual Solid Mechanics conventions, positive tensile stresses/strains are considered, whereas – as is done in Fluid Mechanics – only the isotropic mean pressure is positive if compressive. The usual symbols σ_{ij}, ϵ_{ij}, s_{ij} and e_{ij} are employed to denote the stress tensor, the strain tensor and the corresponding deviatoric components, while $p = -\sigma_{kk}/3$ and $\epsilon_{vol} = \epsilon_{kk}$ are the isotropic mean pressure and the volumetric strain, respectively.

2.1 Drucker-Prager kinematic hardening (DPkh) standard elastic-plastic model

As is well-known, the formulation of constitutive models in the framework of standard hardening elasto-plasticity requires the following ingredients: (i) elastic relationship, (ii) yield function, (iii) plastic flow rule and (iv) hardening law(s).

Under the usual elastic–plastic strain splitting, the incremental linear elastic Hooke's law is expressed as follows:

$$d\sigma_{ij} = D^e_{ijhk}\left(d\epsilon_{hk} - d\epsilon^p_{hk}\right) \tag{1}$$

where d is the differentiation operator, p stands for "plastic" and D^e_{ijhk} is the standard elastic stiffness tensor.

The yield locus $f = 0$ is of the same conical type described by [12, 10]:

$$f = \frac{3}{2}\left(s_{ij} - p\alpha_{ij}\right)\left(s_{ij} - p\alpha_{ij}\right) - k^2p^2 \tag{2}$$

in which α_{ij} is the so-called back-stress ratio tensor and k the yielding parameter. While this latter governs the opening angle of the cone, α_{ij} is a second–rank deviatoric tensor determining the rotation of the yield locus.

The plastic flow rule is in general expressed as:

$$d\epsilon^p_{ij} = d\lambda m_{ij} \tag{3}$$

where $d\lambda$ is the scalar plastic multiplier and m_{ij} rules the direction of the plastic flow. Here the following non–associated flow rule has been adopted:

$$m_{ij} = n^{dev}_{ij} - \frac{1}{3}D\delta_{ij} = \frac{\left(\partial f/\partial\sigma_{ij}\right)^{dev}}{\|\left(\partial f/\partial\sigma_{ij}\right)^{dev}\|} - \frac{1}{3}D\delta_{ij} \tag{4}$$

where the deviatoric unit tensor n^{dev}_{ij} is obtained from the deviatoric component of the yield function gradient (associated deviatoric plastic flow) and D represents the so-called dilatancy coefficient, expressed as suggested by suggested by [10]:

$$D = \xi\left(\alpha^d_{ij} - \alpha_{ij}\right)n^{dev}_{ij} = \xi\left(\sqrt{\frac{2}{3}}k_d n^{dev}_{ij} - \alpha_{ij}\right)n^{dev}_{ij} \tag{5}$$

The definition (5) introduces two further constitutive parameters, namely k_d and ξ: the former relates to the stress obliquity for the transition from contractive to dilative responses; the latter quantitatively governs the volumetric plastic strain rate.

Finally, the evolution law for the back-stress tensor α_{ij} is given according to the well-known Armstrong-Frederick approach [1] (see also [10]):

$$d\alpha_{ij} = \frac{2}{3} h_a de^p_{ij} - c_r \alpha_{ij} \sqrt{\frac{2}{3} de^p_{rs} de^p_{rs}} \tag{6}$$

where h_a and c_r are two hardening constitutive parameters. The incremental relationship (6) yields a saturation–type evolution and the existence of a limit back–stress ratio α^{lim}_{ij} measured by the following tensor norm:

$$\left\| \alpha^{lim}_{ij} \right\| = \sqrt{\frac{2}{3}} \frac{h_a}{c_r} \tag{7}$$

Accordingly, all the feasible stress states lie within an outer surface determined both by α^{lim}_{ij} and the opening parameter k in (2). The external bounding locus is in this case a Drucker–Prager (Lode angle-insensitive) cone: the limit stress obliquity M can be derived for triaxial loading conditions and shown to be equal to $M = k + h_a/c_r$ (both in compression and extension). As a consequence, the material shear strength is ruled by the ratio h_a/c_r, whereas c_r determines the evolution rate of α_{ij}.

2.2 Drucker-Prager kinematic hardening bounding surface (DPbs) model with vanishing elastic region

The DPbs constitutive relationship being presented is in essence a frictional effective–stress update of the cohesive model by [2] (improving the former work by [5]). While an exhaustive description is given in [11], the key-points of the analytical formulation are hereafter reported.

The DPbs model is chiefly characterized by the introduction of a vanishing elastic region: as a consequence, while the same Hooke's elastic law (1) is still used, plastic/irreversible strains take place at the very onset of loading (as is pointed out by many experimental evidences).

Starting from the same yield function definition (2), the following relationship ensures mutually consistent evolutions of the stress state and the back-stress when $k \to 0$:

$$\lim_{k \to 0} f = 0 \Rightarrow s_{ij} = p\alpha_{ij} \Rightarrow ds_{ij} = d\alpha_{ij} p + \alpha_{ij} dp \tag{8}$$

The same plastic flow relationships (3), (4) and (5) are employed for the DPbs model as well, with the exception of the manner in which the deviatoric unit tensor n^{dev}_{ij} is obtained. Specifically, the combination of a Prager-type translation rule for α_{ij} ($d\alpha_{ij} = \|d\alpha_{ij}\| n^{dev}_{ij}$) with the constraint (8) leads to:

$$n^{dev}_{ij} = \frac{ds_{ij} - \alpha_{ij} dp}{\|ds_{ij} - \alpha_{ij} dp\|} \tag{9}$$

Since the direction of the deviatoric plastic strain increment ($de^p_{ij} = d\lambda n^{dev}_{ij}$) depends on the stress increment through n^{dev}_{ij}, the model is intrinsically – and spontaneously – "hypoplastic" [6].

As was done by [2], an incremental hardening relationship is here directly established between the increments of the deviatoric second invariant q and the incremental deviatoric plastic strain (see [11]):

$$dq = \sqrt{\frac{2}{3}} H \| de^p_{ij} \| \tag{10}$$

where H is the so-called hardening modulus. Following a typical bounding surface plasticity approach, H is related to the tensorial distance between the current stress state and its projection onto an *ad hoc* bounding locus $f_{bs} = 0$. In particular, provided a Drucker-Prager bounding locus (set $\|\alpha_{ij}\| = 0$ and $k = M$ in (2)), the hardening modulus is given by:

$$\begin{aligned} H &= p\left(h\beta^m\right) \\ \beta \in \mathbb{R}^+ : \frac{3}{2}\bar{s}_{ij}\bar{s}_{ij} - M^2\bar{p}^2 &= 0, \\ \bar{\sigma}_{ij} &= \sigma_{ij} + \beta\left(\sigma_{ij} - \sigma^0_{ij}\right) \end{aligned} \tag{11}$$

in which h and m are two hardening parameters, whereas σ^0_{ij} embodies the stress tensor at the last load reversal. Since a standard yield locus is missing, the loading/unloading criterion is alternatively defined according to the approach by [2]: to ensure an instantaneous elastic response at the onset of unloading, σ^0_{ij} is set equal to the current stress tensor whenever $d\beta > 0$, so that $\sigma^0_{ij} = \sigma_{ij} \Rightarrow \beta \to \infty$ and therefore $H \to \infty$. In contrast, the fulfilment of $\lim_{\beta\to 0} H = 0$ guarantees the occurrence of failure when the distance coefficient β is nil.

A notable flexibility stems from the fact that the $H\left(\beta\right)$ relationship can be modified without affecting the analytical structure (and the computer implementation), so that the DPbs model can be in principle adapted to reproduce a large variety of experimental results.

2.3 Constitutive parameters and calibration

Both the above models require the calibration of seven constitutive parameters. Two material constants – e.g. the Young modulus E and the Poisson's ratio ν – are needed to characterize the elastic behaviour, usually investigated by means of *in situ* tests and/or laboratory dynamic tests at very small strains.

Then, the two parameters ξ and k_d must be identified to describe the soil volumetric behaviour for a given relative density – or for a narrow range around the calibration value (the use of any density-dependent state parameter has been here avoided for the sake of simplicity).

The remaining three parameters can be set on the basis of a single datum concerning the shear strength (friction angle) and, for instance, the modulus reduction and damping curves (these are in many cases the only available information concerning the cyclic response). In the DPbs model the shear strength is independently governed by the M parameter (opening of the bounding surface), so that the hardening parameters h and m can be selected to get the best match between numerical and experimental cyclic curves. In contrast, hardening and failure properties are not decoupled in DPkh case, this implying the need for a simultaneous identification of k, h_a and c_r.

2.4 Coupling frictional and viscous energy dissipations

The dissipative performance of an elastic-plastic model can be improved via an additional viscous damping mechanism. This means that the global stress state on the soil solid skeleton

can be split into two parallel components ($\sigma_{ij} = \sigma^f_{ij} + \sigma^v_{ij}$), namely a frictional contribution σ^f_{ij} given by thr elastic-plastic behaviour and a viscous term σ^v_{ij}, e.g. of the following form:

$$\sigma^v_{ij} = D^v_{ijhk}\dot{\epsilon}_{hk} \tag{12}$$

where the dot stands for time derivation and D^v_{ijhv} is the fourth-rank tensor of viscous moduli. In standard finite element computations, the additional viscous mechanism (12) is often introduced through the following calibration of the so-called Rayleigh parameters [4] for the damping matrix $\mathbf{C}$:

$$\mathbf{C} = a_0\mathbf{M} + a_1\mathbf{K}^e, \qquad a_0 = 0 \qquad a_1 = \frac{2D_{min}}{\omega} \tag{13}$$

ensuring a damping ratio D_{min} for a given circular frequency ω at very small strains. As could be readily shown [3, 11], the main effects of coupling frictional and (linear) viscous dissipations are: (i) an apparent smoothing of stress-strain loading cycles, avoiding the sharp transitions at stress reversals usually exhibited by purely elastic–plastic responses [3]; (ii) higher material damping, given by the sum of the frictional and the viscous components. While at very low strains the damping ratio approaches the purely viscous limit D_{min}, both the frictional and the viscous components contribute to the global damping at progressively larger strains; suitably, the stiffness modulus reduction results to be unaffected by viscosity.

3 REFERENCE MODULUS REDUCTION AND MATERIAL DAMPING CURVES

The DPkh/DPbs models will be mainly evaluated by comparing their capability of reproducing shear modulus reduction (G/G_{max}) and damping (D) curves. Therefore, reference cyclic curves are needed for the parameter calibration (see section 2.3) and, in this work, the family of normalized curves proposed by Darendeli [7] is taken into account for two reasons: (i) stiffness reduction and damping curves are provided analytically, with particular convenience for their implementation and use in parametric analyses; (ii) the recent development of Darendeli's curves gives sufficient confidence about the absence of "accuracy problems in material damping measurements arising from the use of older generation cyclic triaxial equipment employed in previous studies" [7]. While the reader can refer to the original work [7] for conceptual/operational details, the main aspects concerning the use of Darendeli's curves are hereafter summarized.

As far as the shear modulus reduction is concerned, a modified hyperbolic expression is adopted:

$$\frac{G}{G_{max}} = \frac{1}{1 + (\gamma/\gamma_r)^a} \tag{14}$$

in which γ_r and a are the so-called "reference strain" and "curvature coefficient", respectively. Then, the following relationship for the damping ratio D – defined as usual [9] – is assumed:

$$D = D_{min} + b * \left(\frac{G}{G_{max}}\right)^{0.1} * D_{Masing} \tag{15}$$

where b is a "scaling coefficient", D_{min} the limit damping ratio at very low shear strain ($\lim_{\gamma\to 0} D = D_{min}$) and D_{Masing} the material damping evaluated from the corresponding G/G_{max} trend by assuming the validity of the well-known Masing loading/unloading criterion [9].

The practical use of equations (14) and (15) requires the identification of four material parameters (γ_r, a, b and D_{min}). Based on a significant sample of experimental data, they have been conveniently related to few physical/loading indices through the following empirical formulas:

$$\begin{aligned} \gamma_r &= \left(\phi_1 + \phi_2 * PI * OCR^{\phi_3}\right) * p_0^{\phi_4} \\ a &= \phi_5 \\ D_{min} &= \left(\phi_6\phi_7 * PI * OCR^{\phi_8}\right) * p_0^{\phi_9} * \left[1 + \phi_{10} * ln\left(f\right)\right] \\ b &= \phi_{11} + \phi_{12} * ln\left(N\right) \end{aligned} \tag{16}$$

where:

p_0: mean effective confining pressure [atm]

PI: soil plasticity index [%]

OCR: overconsolidation ratio [-]

f: loading frequency [Hz]

N: number of loading cycles [-]

The values of the twelve constants ϕ_i are not reported here for the sake of brevity but can be found in [7].

4 DPkh and DPbs SIMULATION OF THE SOIL CYCLIC RESPONSE

In this section the cyclic performances of the DPkh and DPbs models are compared by using the above Darendeli's curve as a good analytical approximation of real experimental results. As is implied by Equations (16), G/G_{max} and D damping curves are obtained on the basis of few relevant mechanical/loading parameters. In what follows – unless differently stated – $p_0 = 1$ atm, $OCR = 1$ and $PI = 0$ %, while – as suggested by [7], $f = 1$ Hz, $N = 10$ cycles have been set to approximate typical seismic loading in "single frequency" shear tests.

The plastic volumetric behaviour of the soil is neglected in this study, in order to avoid the complex interaction between soil dilatancy behaviour and the kinematic constraints characterizing many experimental devices [11]. Therefore, the $\xi = 0$ parameter in (5) will be always set to zero (i.e. $d\epsilon_{vol} = 0$), this implying shear strain-controlled cyclic tests to be performed at constant mean pressure $p = p_0$.

While typical values have been selected for the elastic and strength parameters – $E = 10$ MPa, $\nu = 0.25$, $M = 1.2$ (30 deg friction angle), the calibration of the hardening parameters is discussed in more detail, as they mainly affect the resulting G/G_{max} and D curves.

4.1 DPkh simulations

As any standard plasticity model, the DPkh model predicts a purely elastic pre-yielding response and strain-independent cyclic curves for shear strains less than the yielding strain γ_y. Based on this consideration and the above DPkh constitutive equations, the following calibration procedure has been followed:

1. once chosen the amplitude of the elastic range, the opening of the yield locus has been obtained as $k = \sqrt{3\left(G_{max}\gamma_y/p_0\right)^2}$ (the influence of both the elastic shear modulus G_{max} and p_0 should be noted);

2. in order to prescribe a given shear strength M, the hardening and yielding parameters must be related as $h_a = c_r\,(M - k)$;

3. c_r has been varied to modify the overall hardening response.

It is especially worth remarking that, within an elastic-plastic modelling framework, G/G_{max} and D are interdependent: this means that the constitutive parameters must be calibrated to achieve at the same time the best agreement with both the experimental cyclic curves.

In Figure 1 DPkh and Darendeli's curves are compared for two different DPkh yielding strains (γ_y =2.2E-4, 1E-2 %). Darendeli's average curves (blue lines) are given along with the uncertainty ranges derived from the corresponding standard deviations (black dashed lines) [7], while the DPkh D curves have been obtained in both the purely frictional and frictional/viscous versions. The plots in Figure 1 lead to the following conclusions:

- the singularity at the elastic/elastic-plastic transition prevents the DPkh G/G_{max} curves to follow the concavity exhibited by Darendeli's curves;

- the smaller γ_y, the more difficult is to reproduce the experimental trend over the whole strain range. For medium/large γ_y reasonable G/G_{max} ratios are obtained at medium/large strains: this kind of calibration may be acceptable for applications in which the small-strain behaviour (assumed to be linear elastic) is not very important;

- the trend of DPkh D curves is markedly non-monotonic as a consequence of the peculiar interaction between hardening evolution (stiffness degradation) and the cyclic loading/unloading behaviour (determining the shape of the stress-strain cycles);

- the introduction of the parallel viscous mechanism is effective only to reproduce the small-strain damping (neglected by the purely frictional formulation), with no effect on the aforementioned non-monotonicity.

The influence of the hardening behaviour is further explored in Figures 2 and 3, where the simulations in Figure 1 have been repeated for different c_r values (only the purely frictional curves are shown). Expectedly, since c_r governs the shape of the hardening stress-strain branches, it directly affects the decay of the secant shear modulus, as well as the damping ratio. However, regardless of γ_y, obtaining a satisfactory agreement does not appear to be an easy task. Different trends may be obtained by varying at the same time both h_a and c_r, but this would in general modify the prescribed shear strength.

4.2 DPbs simulations

The same Darendeli's curves for $p_0 = 1$ atm have been approximated by using the DPbs model. Figure 4 shows the overall good DPbs performance (much better than the DPkh one), with an almost perfect G/G_{max} match and a qualitatively good agreement in terms of material damping as well. Because of the vanishing yield locus, no elastic/elastic-plastic transition takes place, so that the resulting curves are smooth and easier to be adapted on the experimental trends. However, to author's experience, optimising the agreement in terms of modulus reduction usually prevent very satisfactory damping curves to be obtained. As is shown in Figure 5, better results can be achieved by attempting a "trial-and-error" calibration to reasonably match both G/G_{max} and D curves. Figure 5 also illustrates the beneficial effect of the viscous damping in the small strain range, while it leads to some damping overestimation at larger strains:

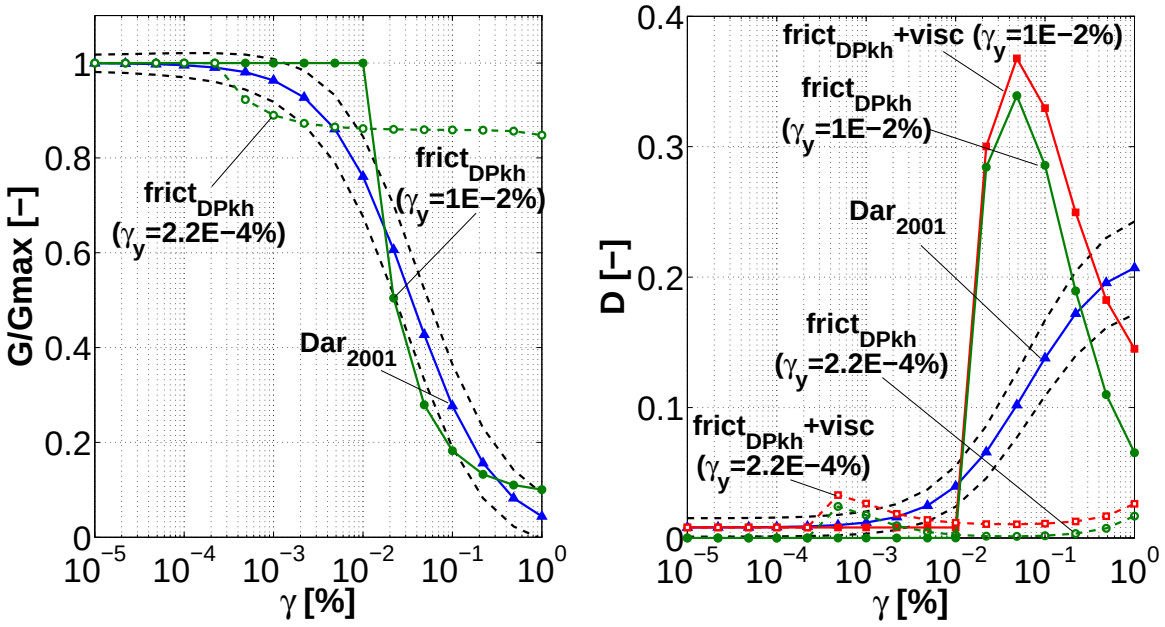

Figure 1: Darendeli-DPkh comparison for $p_0 = 1$ atm and two (γ_y, c_r) couples (γ_y =1E-2% and c_r =10, γ_y =2.2E-4% and c_r =600)

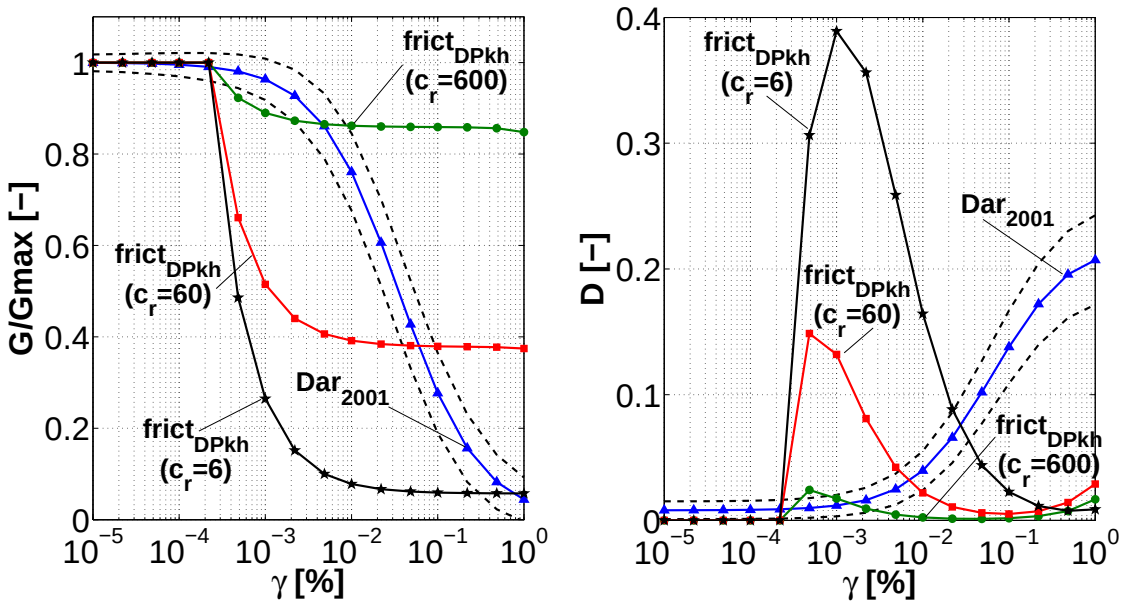

Figure 2: Darendeli-DPkh comparison for $p_0 = 1$ atm, γ_y =2.2E-4% and c_r =6, 60, 600

depending on the specific application, the value of D_{min} can be varied as an additional free parameter to improve the accuracy for a given strain interval.

Figures 6 and 7 exemplify the influence of the hardening parameters h and m, giving the chance to significantly vary the shapes of the predicted curves. Whenever no satisfactory agreement is reached by simply varying h and m, the option of modifying the $H(\beta)$ relationship (11)

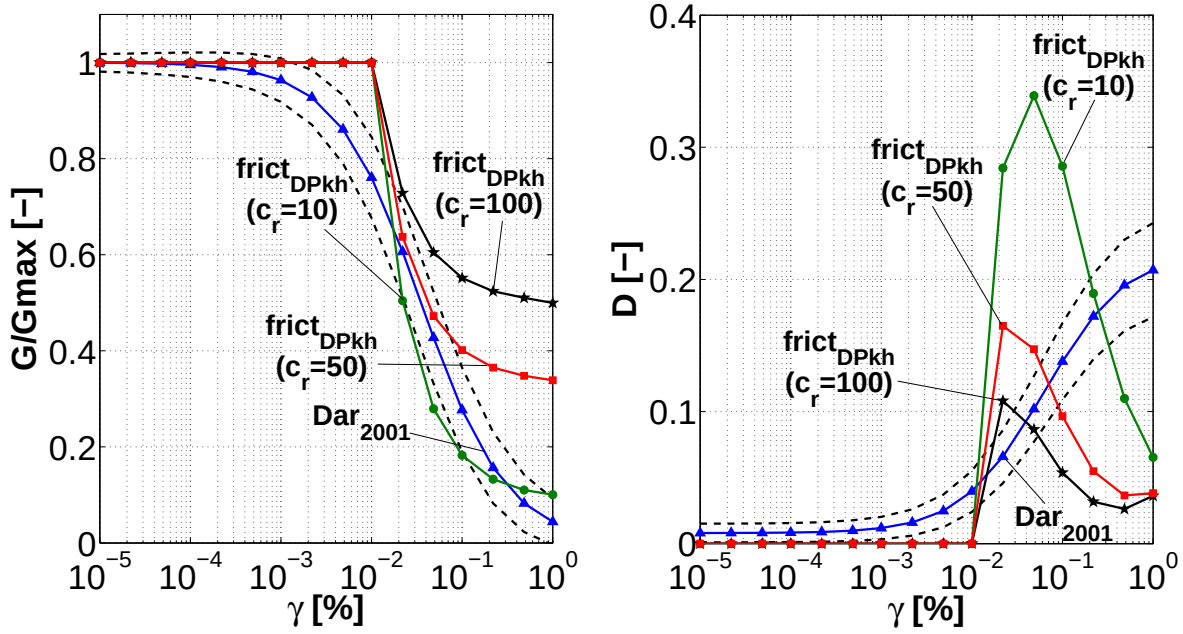

Figure 3: Darendeli-DPkh comparison for $p_0 = 1$ atm, γ_y =1E-2% and c_r =10, 50, 100

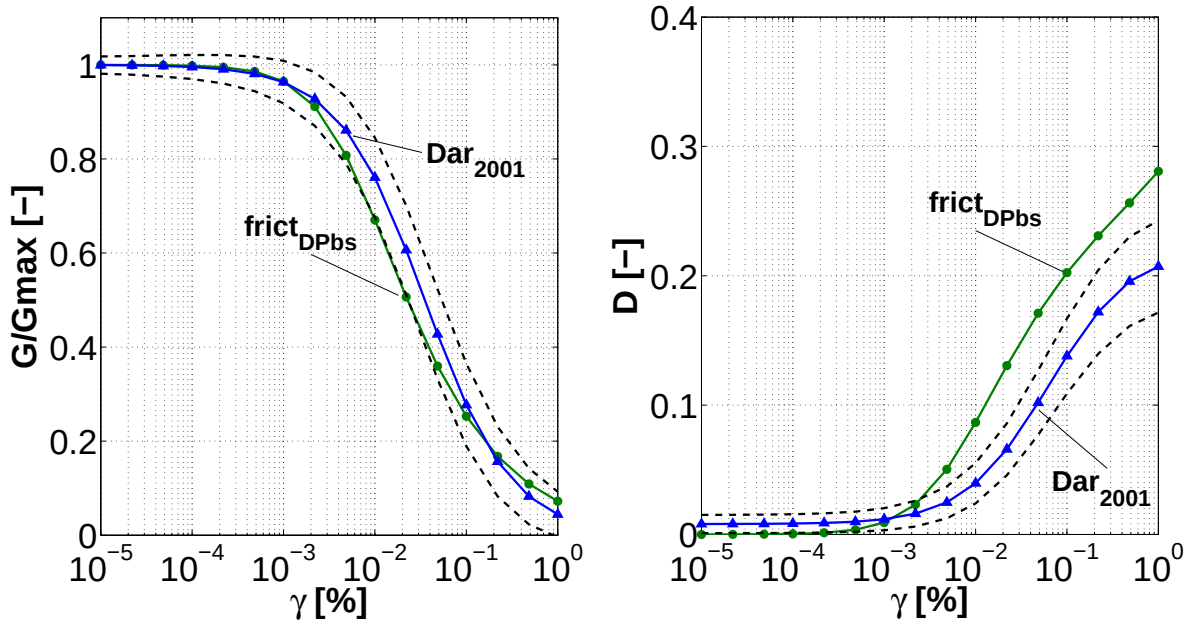

Figure 4: Darendeli-DPbs comparison for $p_0 = 1$ atm (h =0.15, m =1.34)

is always possible with no substantial changes in the structure and the implementation of the model.

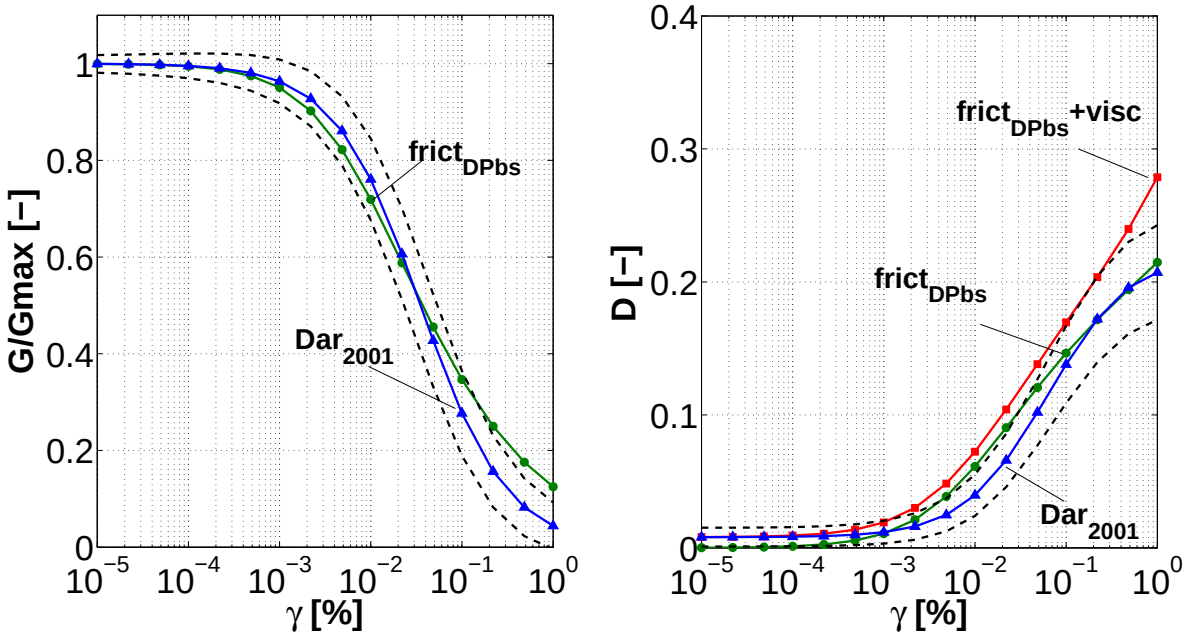

Figure 5: Darendeli-DPbs comparison for $p_0 = 1$ atm (h =1.4, m =1)

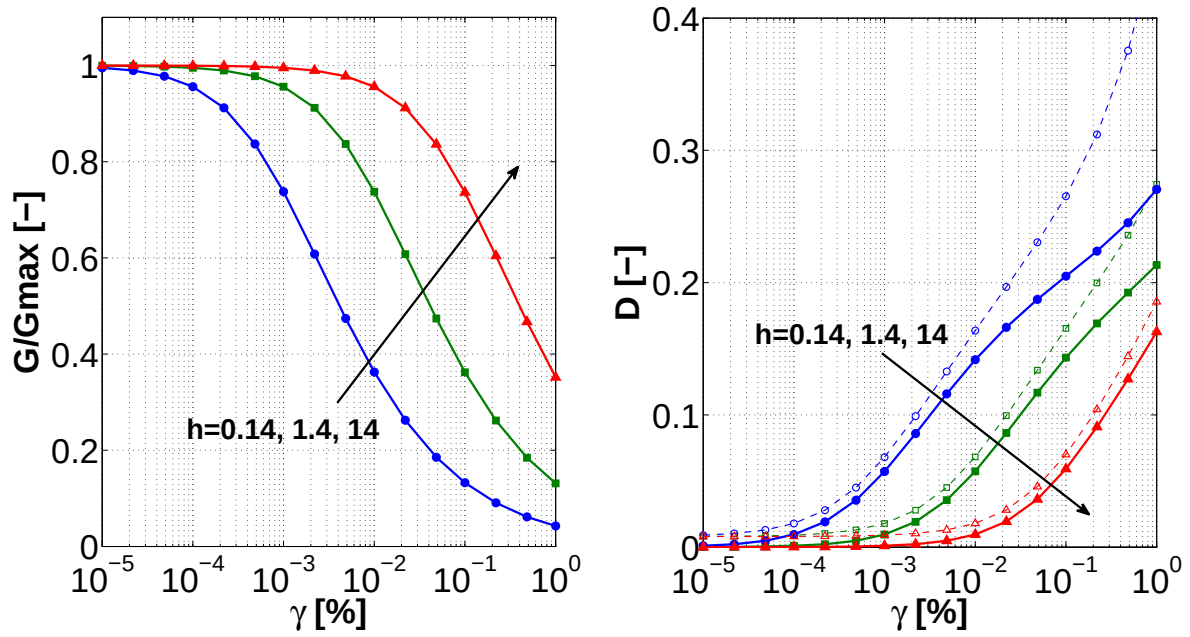

Figure 6: DPbs parametric analyses: $p_0 = 1$ atm, Simulazione 1 atm, m =1, h variable (dashed lines include both frictional and viscous dissipation)

5 DPbs MODELLING OF PRESSURE-SENSITIVE CYCLIC BEHAVIOUR

The mechanical behaviour of frictional materials is considerably pressure-sensitive and, as many experimental evidences confirm, both shear modulus reduction and damping curves are affected by the value of the confining pressure. Accounting for pressure-dependence can be

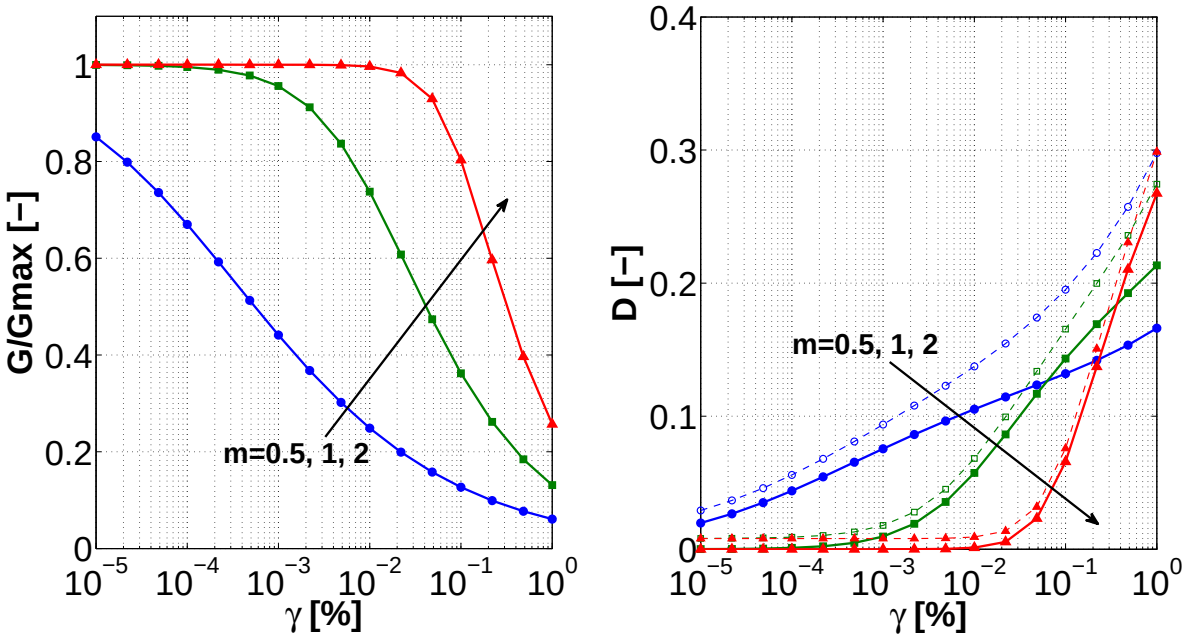

Figure 7: DPbs parametric analyses: $p_0 = 1$ atm, h =1.4, m = variable (dashed lines include both frictional and viscous dissipation)

particularly important in practical applications, especially when the computational soil model involves large depth ranges.

Darendeli's cyclic formulation takes explicitly into account the influence of the initial mean pressure p_0 and can be exploited to check how accurately the DPbs model reproduces this mechanical aspect. Figure 8 illustrates the cyclic pressure-sensitiveness predicted by Darendeli's formulas over the 0.25–16 atm pressure range for the values $OCR = 1$, $PI = 0\%$, $f = 1$ Hz and $N = 10$ cycles. The same simulations have been performed by using the DPbs model and the corresponding outcomes plotted in Figure 9 (frictional mechanism only). As is evident, the DPbs model calibrated for $p_0 = 1$ atm (the material parameters are given in the figure caption) overestimates the effect of the confining pressure and a rather unsatisfactory Darendeli-DPbs agreement results.

A possible simple approach to improve the DPbs performance over a wide pressure range is to introduce p_0-dependent hardening parameters and small-strain damping, requiring two or more calibrations for h, m and D_{min}[1]. Here, four distinct (h, m, D_{min}) triplets have been first set for $p_0 = 0.25, 1, 4, 16$ atm on the basis of Darendeli's formulas and then the following interpolating power laws have been identified:

$$\begin{aligned} h &= 1.2762 * p_0^{-1.95} \\ m &= 0.9952 * p_0^{0.0691} \\ D_{min} &= 0.008 * p_0^{-0.29} \end{aligned} \tag{17}$$

Owing to the convenient formulation of the DPbs model, the introduction of pressure-dependent hardening parameters does not imply any additional analytical/computational difficulty, so that

[1]the pressure-dependence of the elastic moduli has been neglected with no substantial effect on the suitability of the approach proposed

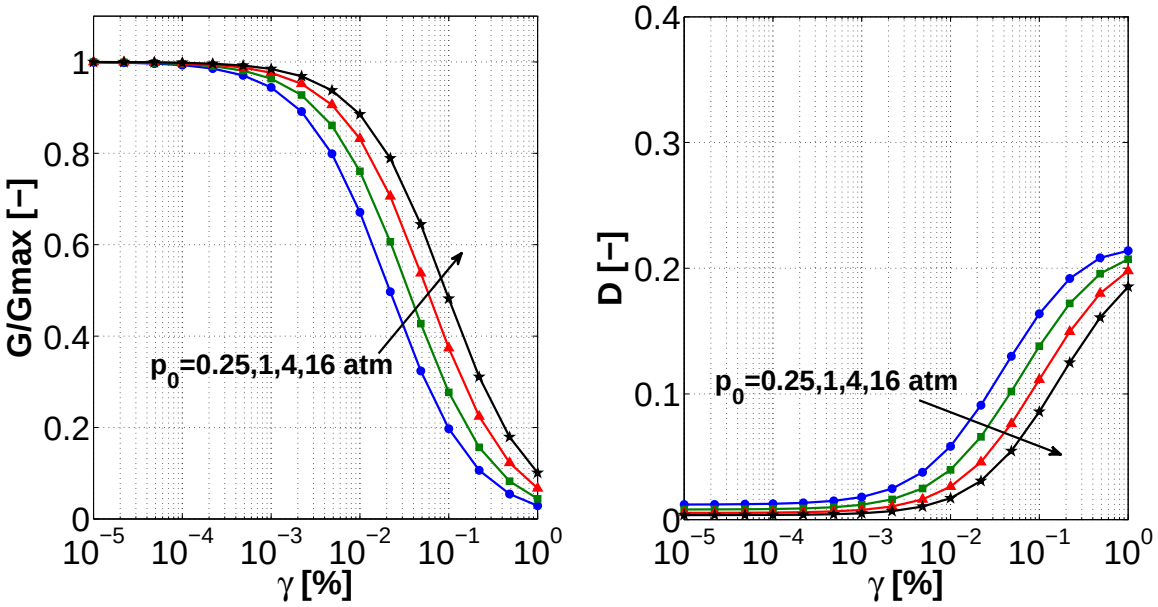

Figure 8: Pressure-sensitiveness of G/G_{max} and D curves predicted via Darendeli's formulas

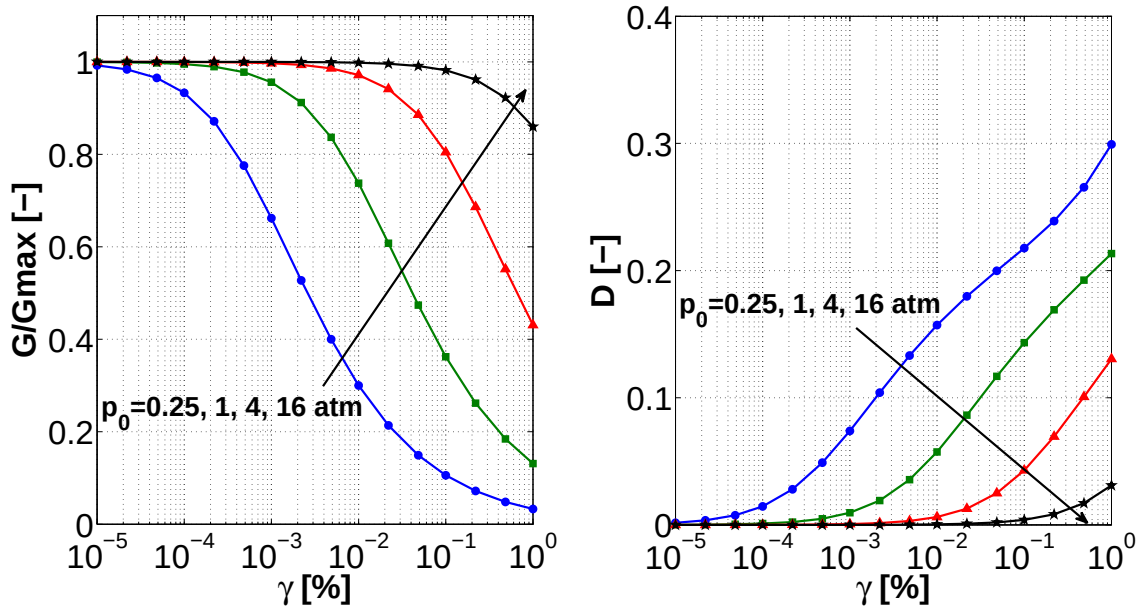

Figure 9: Pressure-sensitiveness of G/G_{max} and D curves predicted via the DPbs model with constant hardening parameters ($E = 10$ MPa, $\nu = 0.25$, $M = 1.2$, $h = 1.4$, $m = 1$)

this slight modification can be readily implemented. Provided the satisfactory Darendeli-DPbs agreement – here not shown – at the calibration pressures ($p_0 = 0.25, 1, 4, 16$ atm), the effectiveness of the interpolation procedure is proven in Figure 10 for the different pressure $p_0 = 8$ atm. Even in this case the contribution of the viscous mechanism is particularly needed at medium/low strains, while it leads to some damping overestimation at higher strain levels: as in the previous cases, some adjustment is possible to get a reasonable match over the whole strain

range.

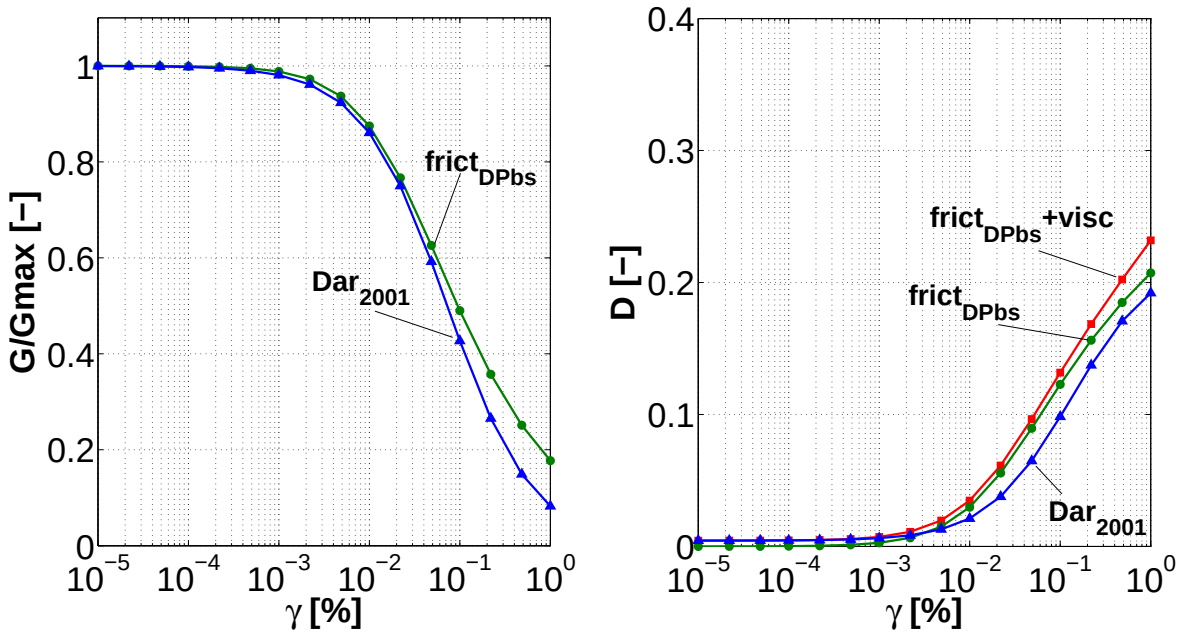

Figure 10: Comparison between Darendeli's and DPbs cyclic curves for $p_0 = 8$ atm

6 CONCLUSIONS

Two elastic-plastic kinematic hardening Drucker-Prager models were formulated and compared in terms of cyclic performance, i.e. simulation of the modulus reduction and damping curves usually employed in the GEE practice. While the former model (DPkh) is a standard elastic-plastic with an Armstrong-Frederick evolution law for the back-stress tensor, the latter (DPbs) was developed within the framework of bounding surface plasticity with vanishing elastic region.

For practical purposes, both the models were formulated by using the same low number of constitutive parameters and including the most essential mechanical characteristics of frictional materials, i.e. pressure-sensitive shear strength and non-associated plastic flow. Despite the apparent similarities, the two models produce very different outcomes and highlight that passing from standard 1D visco-elastic approaches to multiaxial plasticity modelling requires attention on the choice of the specific elastic-plastic framework. Specifically, the DPbs bounding surface approach appeared to work much better than the DPkh one, owing to the absence of the usual elastic/elastic-plastic transition and the easily modifiable relationship for the hardening modulus. In particular, the latter feature was exploited to introduce pressure-dependent DPbs hardening parameters and thus extend the predictive effectiveness over a wide range of confining pressures. The beneficial effect of introducing an additional viscous damping mechanisms was also explored, allowing to precisely reproduce energy dissipation at very low strains and, in general, to remedy some accuracy lack of the purely frictional model.

Further work is currently in progress to investigate the influence of the modelling framework in dynamic boundary value problems, especially in the presence of hydro-mechanical coupling.

REFERENCES

[1] P. Armstrong, C. Frederick, A mathematical representation of the multiaxial Bauschinger effect. Technical Report RD/B/N/ 731, C.E.G.B., 1966.

[2] R.I. Borja, A.P. Amies, Multiaxial cyclic plasticity model for clays. *Journal of Geotechnical Engineering*, **120**, 1051–1060, 1994.

[3] R.I. Borja, C. Lin, K. Sama, G. Masada Modelling non-linear ground response of non-liquefiable soils. *Earthquake Engineering and Structural Dynamics*, **29**, 63–83, 2000.

[4] A.K. Chopra, *Dynamics of structures. Theory and application to Earthquake Engineering*. Prentice Hall, 2000.

[5] Y.F. Dafalias, E. Popov, Cyclic loading for materials with a vanishing elastic region. *Nuclear Engineering and Design*, **41**, 293–302, 1977.

[6] Y.F. Dafalias, Bounding surface plasticity. I: Matematical foundations and hypoplasticity. *ASCE Journal of Engineering Mechanics*, **112**, 966–987, 1986.

[7] M.B. Darendeli, *Development of a new family of normalized modulus reduction and material damping curves*. Ph.D. thesis, University of Texas at Austin.

[8] C.G. di Prisco, D.M. Wood, *Mechanical behaviour of soils under environmentally-induced cyclic loads*. Springer, 2012.

[9] S.L. Kramer, *Geotechnical Earthquake Engineering*. Prentice Hall, 1996.

[10] M.T. Manzari, Y.F. Dafalias, A critical state two-surface plasticity model for sands. *Géotechnique*, **47**, 255–272, 1997.

[11] F. Pisanò, B. Jeremić , Coupling multiaxial plasticity and viscous dissipation for cyclically loaded granular materials. Submitted to *Soil Dynamics and Earthquake Engineering*, 2012.

[12] J.H. Prevost, A simple plasticity theory for frictional cohesionless soils. *International Journal of Soil Dynamics and Earthquake Engineering*, **4**, 9–17, 1985.

[13] O.C. Zienkiewicz, A.H.C. Chan, M. Pastor, B.A. Schrefler, T Shiomi, *Computational Geomechanics with special reference to Earthquake Engineering* . Wiley and Sons, 1999.